PERFORMANCE OF FULL-DUPLEX NON-ORTHOGONAL MULTIPLE ACCESS WIRELESS NETWORK WITH ENERGY HARVESTING

Do Dac Thiem(1)

(1) Thu Dau Mot University

Corresponding author: thiemdd@tdmu.edu.vn

DOI: 10.37550/tdmu.EJS/2025.02.667

Article Info

Volume: 7
Issue: 2
Jun: 2025
Received: Jan. 3rd, 2025
Accepted: Mar. 30th, 2025
Page No: 683-689

Abstract

Full-duplex non-orthogonal multiple access wireless networks with energy harvesting have the potential to improve spectral efficiency and save energy. However, wireless signals are susceptible to eavesdropping by other devices within their coverage area. This paper studies the security performance of a full-duplex non-orthogonal multiple access wireless network with energy harvesting (FDNOMAWNwEH) over Nakagami-m fading channels. Results show that the total throughput increases as the power of the primary transmitter increases. Similarly, the total throughput also increases as the expected security level or the energy harvester efficiency increases. In addition, there exists a value of the NOMA power division factor that maximizes the total throughput. Furthermore, the results show that the total throughput decreases as the fading severity parameter increases.

Keywords: energy harvesting, full-duplex, Nakagami-m fading, non-orthogonal multiple access, performance analysis

1. Introduction

Advanced wireless networks (5G, 6G) with advantages such as low latency and high data rates make them suitable for various wireless applications (Boudjit et al., 2023; Psaromanolakis et al., 2023). Alongside these benefits are challenges, particularly related to power and bandwidth allocation. The large number of devices used in these networks adds to the engineering challenges. Furthermore, these networks require a high level of information security in communications as well as energy efficiency. Therefore, finding system models that can address multiple objectives simultaneously is essential. This model helps enhance both energy efficiency and spectral efficiency while ensuring communication reliability, with an expanding number of users in the networks. Non-orthogonal multiple access (NOMA) is proposed as a good technical solution to improve spectral efficiency in wireless communication systems, especially in next-generation networks like 6G and beyond (Le-Thanh et al., 2024; Li et al., 2022). NOMA allows for the selection of different power levels for nearby and distant devices, facilitating the detection and elimination of interference. This technique is considered a means to improve system performance. Moreover, energy harvesting (EH) techniques are becoming increasingly popular (Fan et al., 2023; Lian et al., 2023; Do-Dac et al., 2021). NOMA users who harvest radio frequency (RF) energy can achieve high energy efficiency. Additionally, full-duplex (FD) mechanisms significantly improve spectral efficiency (Chen et al., 2023) since FD allows for simultaneous transmission and reception of data. Furthermore, Nakagami-*m* fading channels are flexible and general for modeling wireless channels (Dang-Ngoc et al., 2021; Ashraf et al., 2021, Do-Dac, et al., 2020; Ho-Van et al., 2019). The severity parameter of fading, *m*, is adjusted to model different wireless channels. Examples include m=1 for Rayleigh fading and m=0.5 for one-sided Gaussian fading. Thus, this paper studies the security performance of the FDNOMAWNwEH over perfect Nakagami-*m* fading channels.

2. System model

FDNOMAWNwEH are illustrated in Figure 1. The model includes a transmitter (T) and a receiver (R) belonging to the primary network, while the transmitter (S), the far receiver (F), the near receiver (N), and the eavesdropper (E) belong to the secondary network. The communication of the primary network can be represented as downlink mobile communication. T can be a high-power radio transmitter, such as a radio or television station. S collects energy from T to operate due to its limited energy. S transmits NOMA to F and N, and S is assumed to be a full-duplex device with a single antenna. E is the eavesdropper within the coverage area of the secondary network.

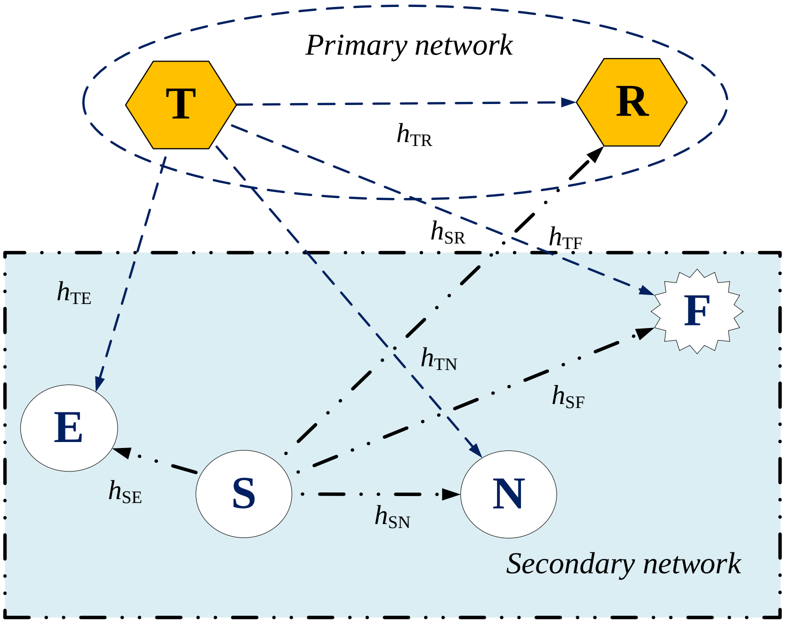

Figure 1. FDNOMAWNwEH model

The channel coefficients between T and R, T and E, T and S, T and N, T and F, S and E, S and S, S and N, S and F, and S and R are denoted as h_{TR}, h_{TE}, h_{TS}, h_{TN}, h_{TF}, h_{SE}, h_{SS}, h_{SN}, h_{SF}, and h_{SR}, respectively. We assume perfect Nakagami-*m* fading links with parameters fading severity and fading power denoted as (m_{ab}, ρ_{ab}), where $a=\{\mathrm{T, S}\}$ and $b=\{\mathrm{R, E, S, N, F}\}$. Furthermore, their probability density function (PDF) and cumulative distribution function (CDF) are provided respectively by

$$F_{|h_{ab}|^2}(y) = \frac{\gamma(m_{ab}, \lambda_{ab} y)}{\Gamma(m_{ab})} \quad (1)$$

$$f_{|h_{ab}|^2}(y) = \frac{\lambda_{ab}}{\Gamma(m_{ab})} y^{m_{ab}-1} e^{-\lambda_{ab} y} \quad (2)$$

where $\lambda_{ab} = \frac{m_{ab}}{\rho_{ab}}$, $\rho_{ab} = \Xi\left\{|h_{ab}|^2\right\} = d_{ab}^{-\tau}$ with d_{ab} is the normalized distance between receiver a and transmitter b.

3. Performance Analysis

a. Signal model

The received signal at S as

$$y_{\mathrm{S}} = h_{\mathrm{TS}}\sqrt{P_{\mathrm{T}}} x_{\mathrm{T}} + h_{\mathrm{SS}}\sqrt{P_{\mathrm{S}}} x_{\mathrm{S}} + \varepsilon_{\mathrm{S}} \quad (3)$$

The energy collected at S as

$$E_{\mathrm{S}} = T\eta\left(P_{\mathrm{T}}|h_{\mathrm{TS}}|^2 + P_{\mathrm{S}}|h_{\mathrm{SS}}|^2\right) \quad (4)$$

The transmitted power of S as

$$\begin{aligned} P_{\mathrm{S}} &= \frac{E_{\mathrm{S}}}{T} = \eta\left(P_{\mathrm{S}}|h_{\mathrm{TS}}|^2 + P_{\mathrm{S}}|h_{\mathrm{SS}}|^2\right) \\ &= P_{\mathrm{T}}|h_{\mathrm{TS}}|^2 / \left(\frac{1}{\eta} - |h_{\mathrm{SS}}|^2\right); \ |h_{\mathrm{SS}}|^2 < \frac{1}{\eta} \end{aligned} \quad (5)$$

The NOMA signal of the secondary transmitter S is x_{S}. Where x_{N} and x_{F} are the separate signals used for N and F respectively, with $\Xi\left\{|x_c|^2\right\} = 1$, $c = \{\mathrm{N}, \mathrm{F}\}$ and μ is the fraction of power allocated to transmit x_{F}. According to the NOMA principle, the x_{F} is allocated more power than the x_{N} and thus $\mu > 0.5$.

$$x_{\mathrm{S}} = \sqrt{\mu P_{\mathrm{S}}} x_{\mathrm{F}} + \sqrt{(1-\mu) P_{\mathrm{S}}} x_{\mathrm{N}} \quad (6)$$

Accordingly, the F, N and E receive the signals y_{F}, y_{N} and y_{E} respectively:

$$y_c = h_{\mathrm{S}c}\sqrt{\mu P_{\mathrm{S}}} x_{\mathrm{F}} + h_{\mathrm{S}c}\sqrt{(1-\mu) P_{\mathrm{S}}} x_{\mathrm{N}} + h_{\mathrm{T}c}\sqrt{P_{\mathrm{T}}} x_{\mathrm{T}} + \varepsilon_c \quad (7)$$

Where ε_c is the noise at c and the noise power is normalized to N_0.

The F first recovers the message x_{F} of F by treating x_{N} as noise and then removing the interference caused by x_{F} before recovering the message x_{N}.

Signal-to-noise plus interference ratio at F as

$$\begin{aligned} \Phi_{\mathrm{F}}^{x_{\mathrm{F}}} &= \frac{\Xi\left\{\left|h_{\mathrm{SF}}\sqrt{\mu P_{\mathrm{S}}} x_{\mathrm{F}}\right|^2\right\}}{\Xi\left\{\left|h_{\mathrm{SF}}\sqrt{(1-\mu) P_{\mathrm{S}}} x_{\mathrm{N}} + h_{\mathrm{TF}}\sqrt{P_{\mathrm{T}}} x_{\mathrm{T}} + \varepsilon_{\mathrm{F}}\right|^2\right\}} \\ &= \frac{\mu P_{\mathrm{S}}|h_{\mathrm{SF}}|^2}{(1-\mu) P_{\mathrm{S}}|h_{\mathrm{SF}}|^2 + P_{\mathrm{T}}|h_{\mathrm{TF}}|^2 + N_0} \end{aligned} \quad (8)$$

Signal-to-noise plus interference ratio at N as

$$\Phi_{\mathrm{N}}^{x_{\mathrm{F}}} = \frac{\Xi\left\{\left|h_{\mathrm{SN}}\sqrt{\mu P_{\mathrm{S}}}x_{\mathrm{F}}\right|^2\right\}}{\Xi\left\{\left|h_{\mathrm{SN}}\sqrt{(1-\mu)P_{\mathrm{S}}}x_{\mathrm{N}} + h_{\mathrm{TN}}\sqrt{P_{\mathrm{T}}}x_{\mathrm{T}} + \varepsilon_{\mathrm{N}}\right|^2\right\}} = \frac{\mu P_{\mathrm{S}}\left|h_{\mathrm{SN}}\right|^2}{(1-\mu)P_{\mathrm{S}}\left|h_{\mathrm{SN}}\right|^2 + P_{\mathrm{T}}\left|h_{\mathrm{TN}}\right|^2 + N_0} \quad (9)$$

The message x_{F} has been decoded successfully, so this interference is eliminated. The received signal at N as

$$\begin{aligned}\tilde{y}_{\mathrm{N}} &= y_{\mathrm{N}} - h_{\mathrm{SN}}\sqrt{P_{\mathrm{S}}}x_{\mathrm{F}} \\ &= h_{\mathrm{SN}}\sqrt{(1-\mu)P_{\mathrm{S}}}x_{\mathrm{N}} + h_{\mathrm{TN}}\sqrt{P_{\mathrm{T}}}x_{\mathrm{T}} + \varepsilon_{\mathrm{N}}\end{aligned} \quad (10)$$

b. Reliability Outage Probability at the far receiver

Given an expected security level C_0, ROP at F is the probability that F fails to decode x_{F} (i.e., the achieved channel capacity of F for decoding x_{F} is less than C_0).

$$\begin{aligned}O_{\mathrm{F}} &= \Pr\left\{log_2\left(1+\Phi_{\mathrm{F}}^{x_{\mathrm{F}}}\right) < C_0\right\} \\ &= \Pr\left\{\Phi_{\mathrm{F}}^{x_{\mathrm{F}}} < \Lambda_0\right\}\end{aligned} \quad (11)$$

where $\Lambda_0 = 2^{C_0} - 1$.

c. Reliability outage probability at near receiver

Conditioned on C_0, ROP at N is the probability that N fails to decode x_{F} or N successfully decodes x_{F} (i.e., the achieved channel capacity of N for decoding x_{F} is higher than C_0) but N fails to decode x_{N}

$$\begin{aligned}O_N &= \Pr\left\{\log_2\left(1+\Phi_{\mathrm{N}}^{x_{\mathrm{F}}}\right) < C_0\right\} + \Pr\left\{\log_2\left(1+\Phi_{\mathrm{N}}^{x_{\mathrm{F}}}\right) \ge C_0,\ \log_2\left(1+\Phi_{\mathrm{N}}^{x_{\mathrm{N}}}\right) < C_0\right\} \\ &= \Pr\left\{\Phi_{\mathrm{N}}^{x_{\mathrm{F}}} < \Lambda_0\right\} + \Pr\left\{\Phi_{\mathrm{N}}^{x_{\mathrm{F}}} \ge \Lambda_0, \Phi_{\mathrm{N}}^{x_{\mathrm{N}}} < \Lambda_0\right\} \\ &= 1 - \Pr\left\{\Phi_{\mathrm{N}}^{x_{\mathrm{F}}} \ge \Lambda_0, \Phi_{\mathrm{N}}^{x_{\mathrm{N}}} \ge \Lambda_0\right\}\end{aligned} \quad (12)$$

d. Total throughput

The total throughput is defined as

$$\tilde{\Theta} = \left(\Theta_{\mathrm{N}} + \Theta_{\mathrm{F}}\right) \quad (13)$$

where throughput at c, Θ_c, is derived from the outage probability analysis as

$$\Theta_c = C_0\left(1 - O_c\right) \quad (14)$$

Obviously, the total throughput of the proposed model depends on throughputs Θ_c. These throughputs are jointly influenced by a set of parameters $\left(P_T, R_0, \eta, \mu\right)$. So, this set affects $\tilde{\Theta}$. Therefore, azchieving the target total throughput requires tuning this set within their feasible range of values.

4. Illustrative results

To obtain the survey data, the nodes are assumed to have random coordinates as follows T(0.4,1.0), R(0.8, 0.9), S(0.1, 0.1), F(0.8, 0.3), N(0.3, 0.1), and E(0.0, 0,4). Normalized distance is used here to simplify the simulation and calculations. Matlab software is used to write the Monte Carlo simulation program with the number of transmission channel realizations 10^6, path loss exponent $\tau = 2.8$, interference power-to-noise variance ratio I_t/N_0=8 dB.

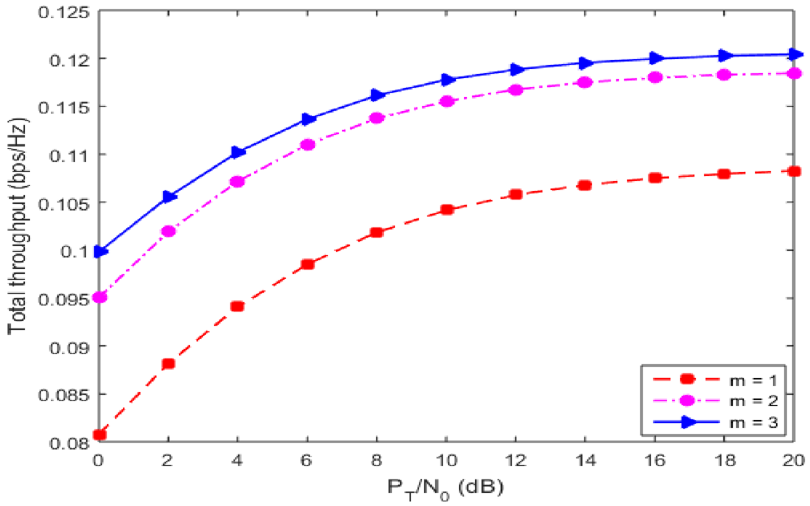

Figure 2. Total throughput versus P_T/N_0 for C_0=0.1bits/s/Hz, $\eta = 0.8$, and $\mu = 0.6$

Figure 2 shows that the total reliable throughput increases as the power of the primary transmitter increases. This is because increasing the power of the primary transmitter enhances the energy harvested at the secondary transmitter. Additionally, this result indicates that the total throughput of the system decreases when the fading severity level is high (with *m* =1). This can be explained by the fact that high fading severity reduces the harvesting capability of the secondary transmitter, leading to lower total throughput compared to when the fading severity is low (*m*=3).

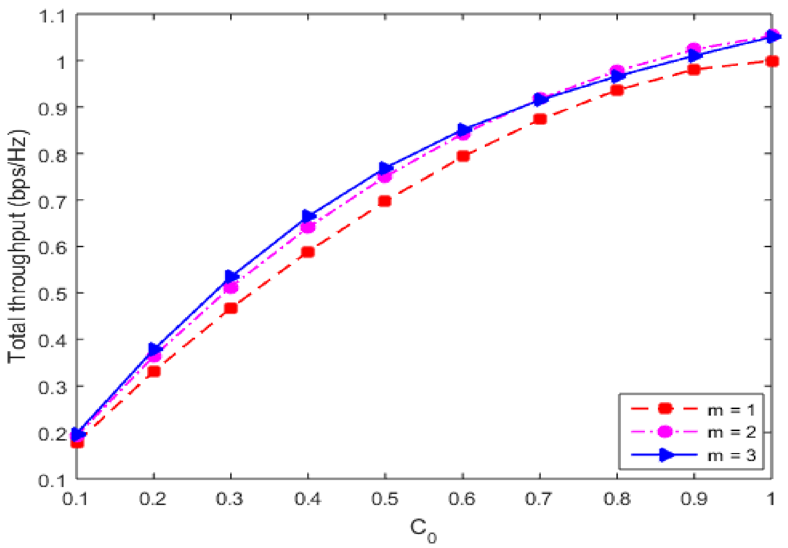

Figure 3. Total throughput versus C_0 for P_T/N_0=15 dB, $\eta = 0.8$, and $\mu = 0.6$

Figure 3 shows that the total throughput increases as the expected security level C_0 increases, meaning that increasing the parameter C_0 helps enhance the performance. Notably, the results indicate that the total throughput reaches a saturation point when C_0 is increased to 1, meaning that further increases in C_0 will not significantly improve performance. With m=1, the throughput is relatively lower compared to the throughput at higher values (m=2 and m=3).

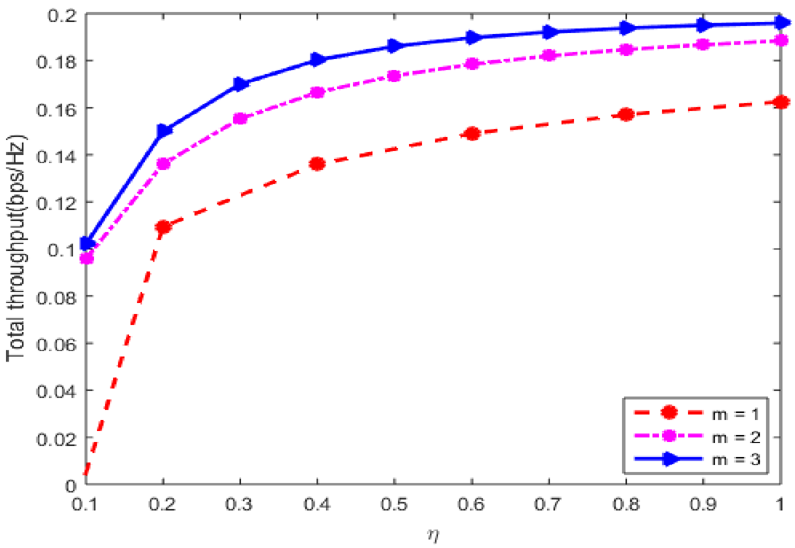

Figure 4. The total throughput versus η for P_T/N_0=15 dB, $\mu = 0.6$, and C_0=0.1bits/s/Hz

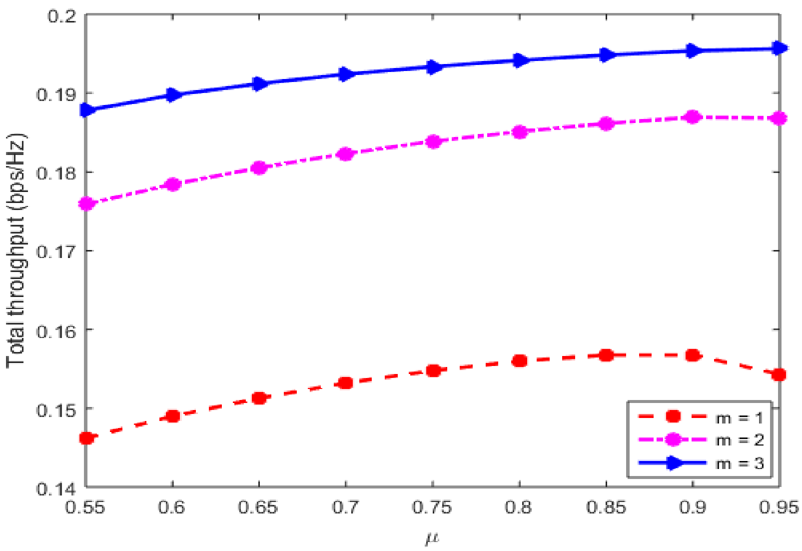

Figure 5. The total throughput versus μ for P_T/N_0=15 dB, $\eta = 0.8$, and C_0=0.1bits/s/Hz

Figure 4 shows that total throughput decreases as energy harvester efficiency η increases. This may indicate that when the system collects energy more efficiently, it can lead to a reduced data transmission capability due to uneven energy distribution or other factors. When the fading severity is low (m=3), throughput tends to decrease less at higher values of η. This suggests that more complex models are capable of maintaining better throughput even when the energy harvesting efficiency is high.

Figure 5 shows that total throughput increases as μ increases from 0.55 to 0.9 (with m=1) but continuing to increase μ will cause total throughput to decrease. This indicates that there exists an optimal value for the power splitting coefficient. As *m* increases, throughput also increases, with more complex models demonstrating better transmission capabilities. This suggests that higher values of *m* can improve performance in power splitting.

5. Conclusions

The results in the paper show that the performance of a full-duplex non-orthogonal multiple access wireless network with energy harvesting over Nakagami-m fading channels is presented in terms of the specific total throughput parameters as follows: When the parameters of the primary transmitter power, the desired security level, and the energy harvesting efficiency increase, the total throughput increases. Meanwhile, the power partition coefficient in the adjustable range exists a value where the throughput reaches its maximum value. Furthermore, the results show that the total throughput decreases when the fading level parameter increases.

References

Ashraf, U. et al., (2021). Performance Evaluation of Nakagami-m Fading with Impulsive Noise. *IET Communication*, 15, 364-373.

Boudjit, S. et al., (2023). End-to-End 5G Priority Scheduling Strategy for a WBAN Health Monitoring System. *In Proc. IEEE WiMob*, Montreal, QC, Canada, pp. 116-122.

Chen, Y. et al., (2023). Next-Generation Full Duplex Networking Systems Empowered by Reconfigurable Intelligent Surfaces. *IEEE Transactions on Wireless Communications*.

Dang-Ngoc, H et al., (2021). Secrecy Analysis of Overlay Mechanism in Radio Frequency Energy Harvesting Networks with Jamming under Nakagami-*m* fading. *Wire. Pers. Commun.*, 120, 447-479.

Do-Dac, T. et al., (2020). Spectrum Sharing Paradigm under Primary Interference and Nakagami-m Fading: Security Analysis. *Wire. Pers. Commun.*, 111, 16071623

Do-Dac, T. et al., (2021). Energy Harvesting Cognitive Radio Networks: Security Analysis for Nakagami-m Fading. *Wire. Netw*, 27, 1561-1572.

Fan, Z. et al., (2023). A Highly Efficient Auto-Polarity Energy Harvesting Circuit Based on Re-configurable TEG Array for Wearable Applications. *In Proc. IEEE ISCAS*, Monterey, CA, USA, pp. 1-4

Ho-Van, K. et al., (2019). Security Analysis for Underlay Cognitive Network with Energy Scavenging Capable Relay over Nakagami-m Fading Channels. *Wire. Commun. and Mobi. Comp.*, Article ID 5080952, pp. 1-16.

Le-Thanh, T. et al., (2024). NOMA MIMO Communications with Harvested Energy: Performance Evaluation. *ETRI Journal*, *46*(3), 432-445.

Li, J. et al., (2022). On the Performance of NOMA Systems With Different User Grouping Strategies. *IEEE Wireless Communications*, *31*(1), 56-61.

Lian, W. X. et al., (2023). A Fully-Integrated CMOS Dual-Band RF Energy Harvesting Front-End Employing Adaptive Frequency Selection. *IEEE Access*, 11, 74121-74135.

Psaromanolakis, N. et al., (2023). MLOps meets Edge Computing: an Edge Platform with Embedded Intelligence towards 6G Systems. *In Proc. IEEE EuCNC/6G Summit*, Gothenburg, Sweden, pp. 496-501.